

Article

Quantitative Description of Duplex Stainless Steels Microstructure Using Selective Etching

Aleksandr Sergeevich Fedorov , Andrey Igorevich Zhitenev *, Darya Andreevna Strekalovskaya, Aleksandr Aleksandrovich Kur and Alexey Aleksandrovich Alkhimenko

Institute of Advanced Engineering Technologies, Peter the Great St. Petersburg Polytechnic University, 195251 St. Petersburg, Russia; fedorov_as@spbstu.ru (A.S.F.); strekal_da@spbstu.ru (D.A.S.); kur_aa@spbstu.ru (A.A.K.); 9586435@mail.ru (A.A.A.)

* Correspondence: zhitenev_ai@spbstu.ru

Abstract: The properties of duplex stainless steels (DSSs) depend on the ferrite–austenite ratio, on the content of secondary phases and on the contamination with non-metallic inclusions. To assess the quality of DSSs, it is necessary to use an integrated approach which includes controlling for the volume fraction, the morphology and the distribution of all phases and non-metallic inclusions. Samples of several grades of DSSs were obtained using various heat treatments, such as solution annealing and quenching from 1050 to 1250 °C to obtain different amounts of ferrite and to provoke annealing at 850 °C to precipitate σ -phase. As a result, a metallographic technique of phase analysis in DSSs based on selective etching and subsequent structure parameters estimation according to ASTM E1245 was developed. We demonstrated that the developed method of quantitative analysis based on selective etching and metallographic analysis according to ASTM E1245 allows us to obtaining much more accurate results, compared to the point count method described in ASTM E562 and to the XRD method.

Keywords: duplex stainless steel; δ -ferrite; austenite; σ -phase; etching; quantification



Citation: Fedorov, A.S.; Zhitenev, A.I.; Strekalovskaya, D.A.; Kur, A.A.; Alkhimenko, A.A. Quantitative Description of Duplex Stainless Steels Microstructure Using Selective Etching. *Metals* **2021**, *11*, 1750. <https://doi.org/10.3390/met11111750>

Academic Editors: Eric D. van Hullebusch, João Pedro Oliveira, Belén Díaz Fernández, Leszek Adam Dobrzański, Jae-chun Lee and Alex Lanzutti

Received: 30 September 2021
Accepted: 27 October 2021
Published: 31 October 2021

Publisher's Note: MDPI stays neutral with regard to jurisdictional claims in published maps and institutional affiliations.



Copyright: © 2021 by the authors. Licensee MDPI, Basel, Switzerland. This article is an open access article distributed under the terms and conditions of the Creative Commons Attribution (CC BY) license (<https://creativecommons.org/licenses/by/4.0/>).

1. Introduction

Recently, the oil and gas and chemical process industries have been experiencing an acute shortage of advanced materials capable of providing reliable and long-lasting solutions [1,2]. The use of traditional materials leads to failures and breakdowns of expensive equipment. The introduction of advanced duplex stainless steels (DSSs) of various grades—depending on the purpose of the steel—can solve this problem [3]. Properties of duplex stainless steels depend on the ferrite-austenite ratio, on the content of secondary phases and on contamination with non-metallic inclusions [4,5]. Currently, it is difficult to obtain metal of the required quality using traditional methods of melting and casting. One of the high-quality steels production methods—the process of electroslag remelting (ESR) after induction melting—provides refining of the remelted metal, which results in a low content of detrimental impurities, but at the same time is quite expensive. When choosing the optimal technology, induction melting is a more effective method which allows us to obtain a homogeneous metal with a low content of non-metallic inclusions at a lower cost.

To assess the quality of DSSs, it is necessary to use an integrated approach, including control of the volume fraction, morphology, distribution patterns of all phases and non-metallic inclusions. The actual phase content depends on the chemical composition of the steel and the heat treatment of the final product [6,7]. Existing physical methods of assessing phases volume fractions, such as magnetic response or X-ray diffraction (XRD) quantitative phase analysis, work either with reference to certain databases to interpret the results or in very narrow determination ranges [8–10]. These methods also require preparation of additional specimens, while metallographic assessment can be carried out using specimens made for mechanical tests. There is a wide range of metallographic

standards and methods for assessing grain size [11], non-metallic inclusions content [12] and microstructural banding [13] for carbon steels. However, there are only a few such standards for DSSs. Therefore, the purpose of this paper is to study the applicability of existing and successfully used metallographic analysis methods for DSSs, as well as the development of new methods based on them, taking into account the specifics of DSSs.

2. Materials and Methods

The specimens of several grades of cast duplex steels were investigated (Table 1). The specimens were examined both in the as-cast and after-heat treatments. Steels 1, 2, and 3 were produced in the laboratory open induction furnace [14]. The raw materials were high-purity electrical steel, metallic Cr, metallic Ni, FeMn-95, and FeMo-60. After heating and melting at 1485 °C, liquid steel was poured into a cylindrical copper mold of 40 mm in diameter and 100 mm in height. The chemical composition of experimental steels was analyzed using spark optical emission spectroscopy. The content of sulfur and phosphorus in all steels did not exceed 0.01%. Steel 4 and Steel 5 were produced in the industrial induction furnace.

Table 1. Chemical compositions of experimental steels.

Steel	PREN *	Element, wt. %								
		C	Si	Mn	Ni	Mo	N	Cu	Ti+Nb+V	Cr
1	24									21
2	26	0.02	0.6	1.6	6.0	0.5	0.04	0.17	0.060	23
3	29									26
4	44	0.03	0.5	1.0	6.0	4.0	0.20	2.50	0.100	23
5	38	0.07	0.6	0.5	8.1	2.9	0.12	0.46	0.027	27

$$* \text{PREN} = (\% \text{Cr} - 14.5\% \text{C}) + 3.3\% \text{Mo} + 2\% \text{W} + 2\% \text{Cu} + 16\% \text{N}.$$

Steel samples were heat treated in the programmable muffle furnace: heated to various temperatures from 1050 to 1250 °C with a step of 50 °C, held at each temperature for 60 min, and quenched in water. In Steel 4 the formation of a σ -phase is possible [15]. Thus, samples of Steel 4 were subjected to annealing at a temperature of 850 °C for 15–120 min to form various amounts of a σ -phase.

Heat-treated steels were used to produce metallographic specimens by molding them in a phenolic compound and polishing. The structures of these specimens were revealed using various etchants.

Metallographic analysis was performed using the light optical microscopy method. The microstructure was investigated using the inverted Reichert-Jung MeF3A microscope (Reichert Inc., Depew, NY, USA) equipped with a Thixomet Pro image analyzer (Thixomet Ltd., St.-Petersburg, Russia). Particles larger than 1 μm were investigated. The confidence level in determining the measurement error was 95%.

The chemical composition of each phase was studied using a Zeiss Supra scanning electron microscope (Carl Zeiss AG, Oberkochen, Germany) equipped with an energy-dispersive spectrometer. The phase content of the specimens was determined using Bruker X-ray diffractometer (Bruker Ltd., Billerica, MA, USA) to confirm the results of quantitative metallography. Thermodynamic modeling was carried out using the ThermoCalc software package (TCW5, Thermo-Calc Software Inc., Solna, Sweden) with the TCFE database [16].

Tests of resistance to crevice corrosion were carried out in accordance with ASTM G48-11, Method B. The specimens were placed inside a beaker and immersed with the FeCl_3 solution for 72 h at 50 °C. Sample surfaces were prepared on 120 grit abrasive paper. Specimens were degreased with acetone, after which cylindrical TFE-fluorocarbon blocks were fastened on them. After the test has been completed, the specimens were cleaned

using a Buehler UltraMet V Ultrasonic Cleaner (Buehler Ltd., Lake Bluff, IL, USA) to remove corrosion products.

Corrosion rate (CR) was calculated using the following Equation (1):

$$CR (\text{g/m}^2 \cdot \text{h}) = \Delta m / S \cdot \tau, \quad (1)$$

where Δm —weight loss (g); S —the surface area of the exposed sample (m^2); τ —immersion time (h).

The pitting potential E_{pit} was determined in accordance with the ISO 17475:2005 as described in [17]. The test cell controlled by a VersaStat Princeton Applied Research (AMETEK Inc., Berwyn, PA, USA) potentiostat was used for measurements. The tests were carried out at the room temperature in a 5% NaCl solution buffered with acetic acid to $\text{pH} = 3$. A silver chloride reference electrode and an additional platinum electrode were used for testing. The linear anodic polarization was carried out using a potentiodynamic mode in the potential range from -250 to 700 mV relative to the corrosion potential E_{cor} with a sweep rate of 0.16 mV/s. The corrosion rate was determined using the obtained polarization curve.

The mechanical properties of the steels were determined by the macrohardness testing using a Zwick/Roel ZHU 8187.5 hardness tester (ZwickRoell GmbH & Co. KG, Ulm, Germany) according to the Vickers method with a load of 10 kg and a holding time of 10 s.

DSSs Etchants Overview

Numerous works are known in which one or another reagent was used [18–22] to reveal the structure of DSSs (Table 2). However, there is no unified approach that allows a sufficiently accurate quantitative assessment of the DSSs' structure. The well-known method for determining volume fraction by systematic manual point count allows measurement of the ferrite or austenite amount even with a low etching quality. Modern image analyzers can significantly increase the accuracy and speed of measurements, provided that an image of the structure is suitable for recognition. Table 2 lists the most common reagents used to identify the structure of DSSs. The articles describe different applications of these reagents. For example, etching with the Murakami etchant was used in [18]; however, in [19] it was shown that it is rather difficult to identify ferrite if its fraction is small when using such etching. Another equally important issue is the selective etching of the σ -phase. The most common method for its recognition is XRD. There is no definite etchant for revealing of a σ -phase [18,19,21] and other harmful phases in DSSs.

Table 2. Used etchants and features of their application.

No.	Name	Composition	Notes	Refs.
Chemical etching				
1	Inhibited ferric chloride	100 mL water, 5 g FeCl_3 , 1 g NaNO_3	Identifies detrimental phases in lean DSSs	[21]
2	Sodium Hydroxide	100 mL water, 40 g NaOH	Identifies detrimental phases	[18]
3	Modified Beraha reagent (Beraha's sulfamic acid reagent No. 4)	100 mL water, 3 g $\text{K}_2\text{S}_2\text{O}_5$, 2 g sulfamic acid, 0.5–1 g $\text{NH}_4\text{F} \cdot \text{HF}$	Identifies phases in high-alloy steels upon immersion for 30–180 s	[21]
4	Beraha reagent	20 mL HCl, 80 mL water, 1 g $\text{K}_2\text{S}_2\text{O}_5$	Reveals ferrite. Etch by immersion until formation of tint	[19,21]
5	Carpenter reagent	85 mL ethanol, 15 mL HCl	Identifies grain boundaries and σ -phase. Etch by immersion for 15–45 min	[19,21]
6	Murakami reagent	100 mL water, 10 g NaOH, 10 g $\text{K}_3\text{Fe}(\text{CN})_6$	Reveals ferrite when heated up to 80 – 100 °C, reveals carbides at room temperature	[19,21]
7	"Glyceregia"	15 mL HCl, 10 mL glycerol, 5 mL HNO_3	Reveals grain boundaries and σ -phase	[18]
Electrolytic etching				
8	HNO_3	60% nitric acid	Identifies ferrite and σ -phase when etched at 2.2 V for 10 s	[20]
9	NaOH	100 mL water, 20 g NaOH	Identifies ferrite and σ -phase when etched at 3 V for 10 s	[21]

3. Results

3.1. Etching Method Development

To develop a quantitative assessment technique, it is necessary to find an etchant that allows obtaining an image with distinguishable phases for automatic analysis. The structure of the Steel 1 specimen with 21% Cr (Table 1) quenched from a temperature of 1200 °C was investigated (Figure 1). Three Vickers indentations were made for investigated area identification after each subsequent etching. A polishing with a minimal metal removal was carried out to always observe the same plane after each etching iteration.

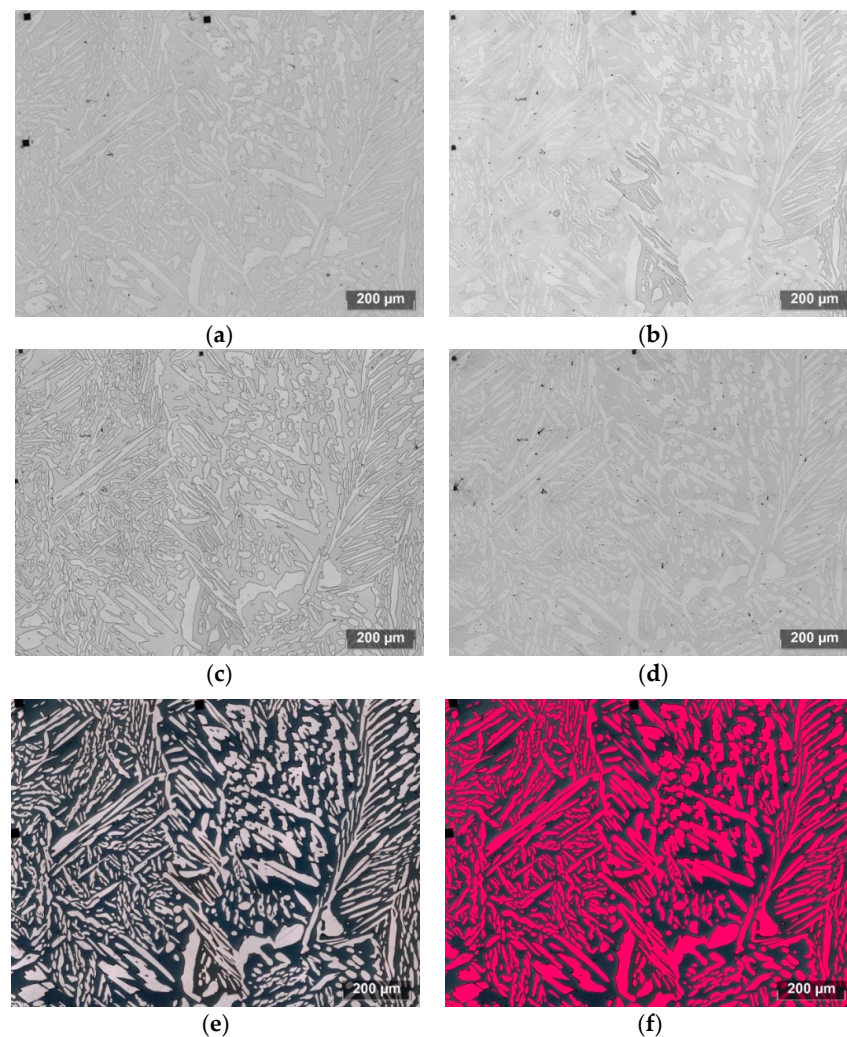


Figure 1. Microstructure of Steel 1 quenched from 1200 °C after electrolytical etching using NaOH (a), chemical etching using Glyceregia (b), Carpenter (c), Murakami's (d), and Beraha's (e) etchant solutions and austenite automatic identification after using Beraha's etchant (f).

Some etchants (reagents 1–3, Table 2) recommended by other authors are not applicable to the investigated DSSs. Thus, the chemical etching with inhibited ferric chloride or with sodium hydroxide did not reveal the structure. The modified Beraha's reagent showed a very indistinguishable structure.

Electrolytic etching is one of the most common techniques for revealing the structure of DSSs [18]. Figure 1a shows a dark ferrite matrix and light austenite areas [23] revealed by electrolytical etching using NaOH etchant. Using 60% nitric acid as an electrolyte provides the same result. This etching method consistently provides high-quality images of the DSSs' structure, but the contrast between phases is insufficient for an automatic classification by

the image analyzer. This etching technique is only suitable for measuring via the manual point count method [24].

Other etchants according to Table 2 (Glyceregia in Figure 1b, Carpenter in Figure 1c, Murakami's etchant in Figure 1d) showed similar results. Similar to electrolytic etching these etchants do not provide sufficient contrast on images for automatic quantitative description of the DSSs' microstructure. The Murakami etchant solution requires heating to a temperature of 80–100 °C, which is unsafe and requires additional equipment.

Etching with Beraha's reagent (solution 4, Table 2) makes it possible to distinguish ferrite (Figure 1e), which is darkened opposed to unetched austenite. The luminosity difference is sufficient to carry out an image binarization and to automatically determine the volume fraction of the phases according to the ASTM E1245 (Figure 1f). The evaluation was carried out on panoramic images with an area of 1.4 mm². To assess the error, a series of preliminary analyzes were carried out, in which it was found that the relative error of measurement by the metallographic method does not exceed 5%.

The approval of the research methodology was carried out on Steels 1–3. Depending on the chemical composition and on the heat treatment of the DSSs, it is possible to obtain different austenite to ferrite ratios and to provoke the σ -phase formation. Taking into account the calculations carried out earlier in [14], a series of heat treatments of experimental steels was carried out (Table 3). The content of δ -ferrite in specimens of the studied steels (Table 1), quenched after holding at different temperatures, was determined using a technique based on etching with Beraha's reagent and subsequent automated image analysis. The measurement results are in good agreement with phase contents predicted by thermodynamic calculations (Table 3 and Figure 2). The XRD analysis results have some inaccuracies. For example, for Steel 1 quenched from 1200 °C, the δ -ferrite content determined using XRD is 77 wt.%, while the automated image analysis and thermodynamic calculations show 57 vol.% and wt.%, respectively. In this case, thermodynamic modeling was used to check the measurement results. In our experiments with prolonged (more than 60 min for 35 g specimens) isothermal holdings, the processes were almost complete and the thermodynamic equilibrium was practically achieved.

Table 3. Comparison of methods for assessing the fraction of phase components by the example of δ -ferrite.

Steel	Quenching Temperature, °C	Automatic Analysis after Etching with Beraha's, vol.%	Measurements by the Systematic Manual Point Count Method after Electrolytic Etching with NaOH, vol.%	XRD (Two Measurements), wt.%	Thermodynamic Modeling, wt.%
1	1050	38.51	35.5	35.9/35.9	32.3
	1100	42.03	37.0	91.5/38.2	38.8
	1150	48.42	46.5	–	47.7
	1200	56.96	52.5	9.5/77.1	57.4
	1250	57.32	46.5	51.6/13.0	69.8
2	1050	56.14	41.5	52.5/52.5	48.1
	1100	62.22	54.0	15.8/58.1	55.0
	1150	72.64	72.5	79.0/77.7	63.3
	1200	81.47	84.5	79.2/82.8	73.2
	1250	85.22	93.0	80.6/80.8	85.0
3	1050	74.04	61.0	43.5/64.2	67.4
	1100	82.79	72.5	59.7/68.7	74.6
	1150	91.06	94.0	–	82.8
	1200	99.86	97.0	100/100	92.1
	1250	99.90	100	100/100	100
4	1050	68.40	–	–	–
	1100	71.17	–	–	–
	1200	82.40	–	–	–
5	1050	48.03	–	–	–
	1100	54.27	–	–	–
	1200	67.67	–	–	–

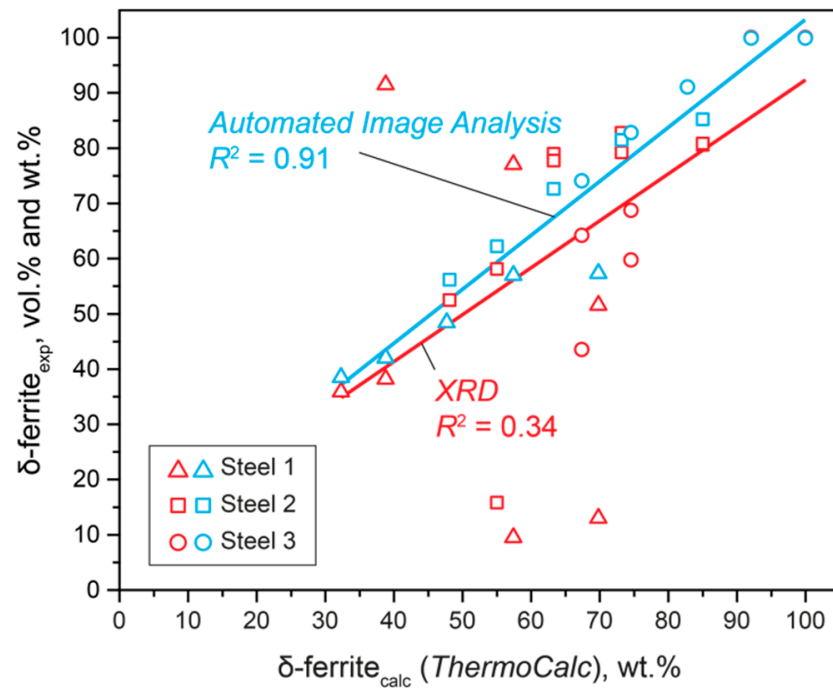


Figure 2. Comparison of phases volume fraction estimation methods.

The σ -phase formation leads to the strengthening of DSSs and to a simultaneous decrease in corrosion properties. Figure 3 shows the microstructure of a Steel 4 specimen after provoke annealing at 850 °C and revealed using the Beraha's reagent (reagent 4, Table 2), which showed the best result discussed earlier in identifying ferrite and austenite.

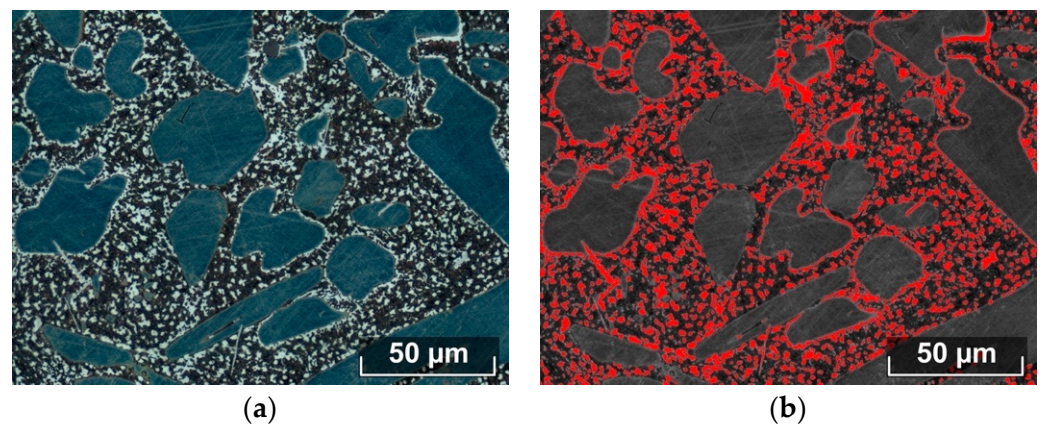


Figure 3. Darkened ferrite, light gray σ -phase, and blue austenite (a) in Steel 4 microstructure after annealing was provoked at 850 °C for 60 min and a phase identification using automated image analyzer (b).

This etching darkens ferrite areas that have not transformed into a σ -phase, light gray areas of the σ -phase, and blue austenite (Figure 3a). The obtained image can be binarized by grayscale threshold and used for the automated phase volume fraction analysis (Figure 3b). Volume fraction of σ -phase (red in Figure 3b) was found.

For a more detailed interpretation of the phase nature, the local chemical compositions were determined (Figure 4 and Table 4).

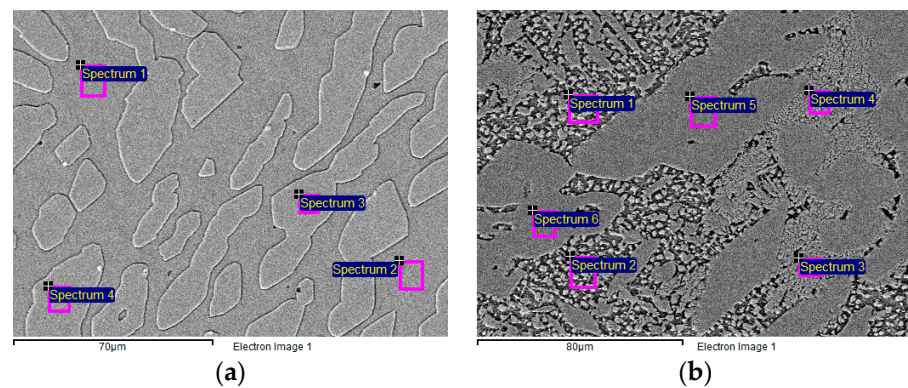


Figure 4. SEM images of ferrite and austenite in: (a) Steel 1 after quenching from 1200 °C; (b) Steel 4 after provoke annealing at 850 °C for 15 min.

Table 4. Chemical composition of phases in DSSs specimens.

No.	Spectrum (Figure 4)	Element, wt. %					Phase
		Cr	Ni	Mo	Mn	Si	
Steel 1, quenched from 1200 °C (to Figure 4a)							
1	1	23.3	5.4	1.9	1.5	0.7	δ
2	2	23.0	5.7	2.5	1.5	0.8	
3	3	20.1	7.5	1.0	1.8	0.7	γ
4	4	20.2	7.2	1.1	1.6	0.7	
Steel 4, quenched from 1050 °C, provoked annealing at 850 °C for 15 min (to Figure 4b)							
5	5	25.0	8.0	4.2	1.4	0.5	γ
6	6	25.0	7.7	4.6	1.4	0.6	
7	3	28.2	5.1	8.0	1.2	0.7	δ
8	4	28.5	5.1	8.1	1.1	0.6	
9	1	25.8	6.2	12.3	1.2	0.6	σ
10	2	26.0	5.8	12.4	1.2	0.7	

The content of ferrite-stabilizing elements in ferrite of Steel 1 quenched from 1200 °C (Figure 4a, Table 4, lines 1, 2) was as follows: 1.9–2.5% Mo, 23.0–23.3% Cr, and 5.4–5.7% Ni. Cr and Mo content in austenite (Figure 4b, Table 4, lines 3, 4) is lower (20.0–20.2% and 1.0–1.1%, respectively). Ni content in austenite is higher than in ferrite and reaches 7.2–7.5%. The content of the remaining elements (Mn and Si) is the same considering the error in their determination. The lowest content of Cr and Mo (25% and 4.2–4.6%, respectively) was determined in the austenite of Steel 4, which was subjected to provoked annealing for precipitation of a σ -phase at 850 °C for 15 min (Figure 4b, Table 4, points 5, 6). Ni content in this steel was found to be the highest. Cr and Mo content in the ferrite (Figure 4b, Table 4, points 7, 8) was higher (28.2–28.5% and 5.1%, respectively). Cr content in the σ -phase (Figure 4b, Table 4, points 9, 10) was slightly lower than in the ferrite, and Mo content was the highest, reaching 12.3–12.4%.

Therefore, the proposed analysis method (etching with Beraha's reagent with subsequent automated image analysis) makes it possible to clearly distinguish austenite, δ -ferrite, and σ -phase in DSSs in images for automatic quantitative assessment according to ASTM E1245.

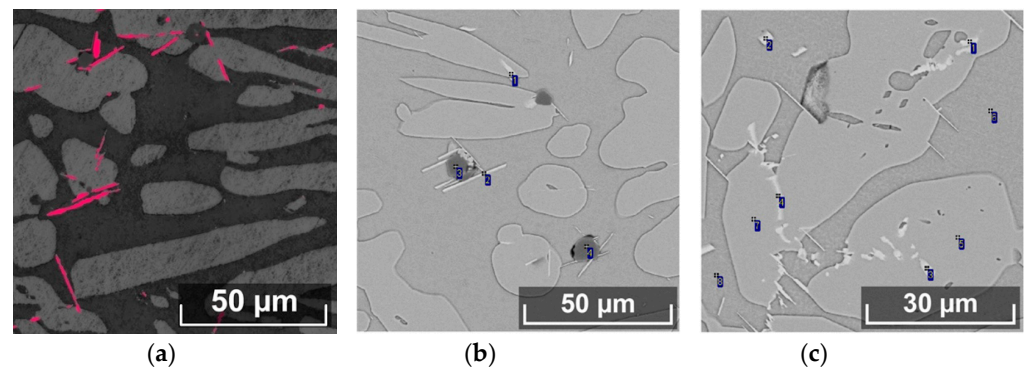
Three specimens of Steel 4 quenched from 1050 °C and subjected to provoked annealing at 850 °C were investigated to verify the method of the σ -phase quantifying. The measurement results shown in Table 5 are consistent with the data on the kinetics of the σ -phase [25]. The σ -phase was completely precipitated in the first 15 min and then its amount remained unchanged.

Table 5. The results of evaluating the amount of the σ -phase in specimens of Steel 4 after provoke annealing at 850 °C.

Holding Time, min	Volume Fraction of the σ -Phase Determined by Automated Image Analysis after Etching with Beraha's Reagent, vol.%	Weight Fraction of the σ -Phase Determined by XRD, wt.%
15	15.56 ± 2.17	23.0
30	14.64 ± 2.07	25.5
60	13.58 ± 1.03	34.1

In addition to the σ -phase the precipitation of other detrimental secondary phases is possible in highly alloyed DSSs with a high PREN. The possibility of recognizing secondary phases using automated image analysis after etching with Beraha's reagent is shown using high-alloy Steel 4 as example.

Secondary phases on the images obtained after etching with the Beraha's reagent were identified accurately using automated image analysis (Figure 5a) and are consistent with the images obtained by SEM (Figure 5b,c). The undesirable secondary phases precipitations in Steel 4 are presented as various morphology particles of Laves phase (long stripes and granules) [26]. The results of secondary phases volume fraction evaluating depending on the quenching temperature are presented in Table 6.

**Figure 5.** Microstructures of Steel 4: (a) secondary phase identification after etching with Beraha's reagent; (b,c) SEM images.**Table 6.** Evaluating the volume fraction of secondary phases in Steel 4.

Quenching Temperature, °C	Volume Fraction of Secondary Phases, vol.%
1050	0.65
1100	0.62
1200	0.54

Violation of the melting conditions leads to the formation of non-metallic inclusions which should be considered when evaluating the quality of DSSs. In addition to assessing the volume fraction of secondary phases, the contamination of the Steels by non-metallic inclusions (NMIs) was assessed on images of unetched specimens (Table 7).

Table 7. Assessment of Steels NMIs contamination.

Steel	Volume Fraction, vol.%	Mean Feret's Diameter, μm	Max Feret's Diameter, μm
1	0.012 ± 0.005	4.8 ± 0.3	9.1
4	0.146 ± 0.027	5.9 ± 0.3	17.2
5	0.214 ± 0.048	7.0 ± 0.5	23.5

Steel 1, produced in the laboratory induction furnace, has 0.012 vol.% of NMIs. Steel 4 and Steel 5, produced in the industrial induction furnace, contain 0.146 vol.% and 0.214

vol.% of NMIs, respectively. The usage of this method and the accumulation of assessment results in different DSSs can become the basis for the development of metal products quality requirements.

3.2. Corrosion Properties

Automated image analysis after etching with the Beraha's reagent made it possible to reliably estimate the amount of δ -ferrite in the steels depending on the quenching temperature, to investigate the impact of the δ -ferrite amount in DSSs on the resistance to pitting and crevice corrosion.

The crevice corrosion rate values of Steels 1, 2, and 3 with a lower PREN are higher than the corrosion rates of Steels 4 and 5. The behavior of the curves obtained for steels with different PRENs is different (Figure 6). For Steels 1, 2, and 3, the crevice corrosion rate values gradually increase from 11 to 14 g/m²·h. Apparently, in steels with a low PREN, crevice corrosion processes are less sensitive to structural changes (the ratio of phase components) than in steels with a high PREN. The crevice corrosion rate increases with distance from the point of equilibrium of δ -ferrite and austenite on phase diagram.

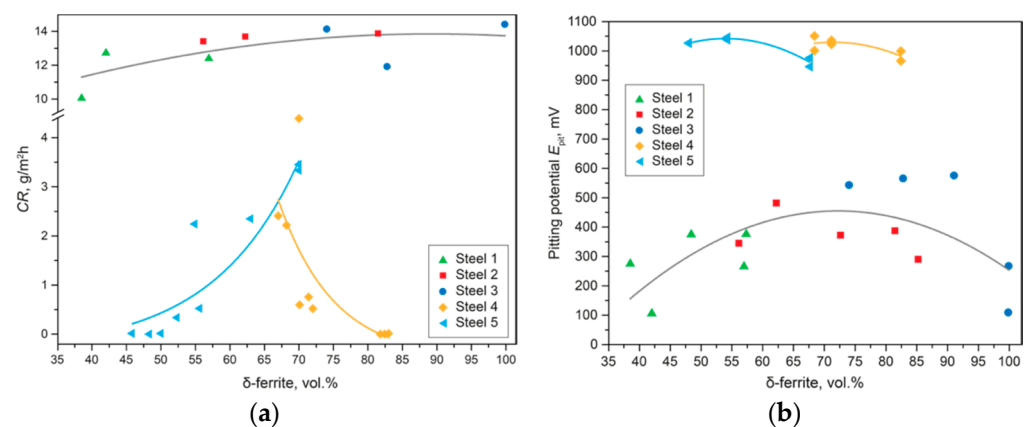


Figure 6. Corrosion properties of the Steels depending on the δ -ferrite content: (a) crevice corrosion rate; (b) pitting potential (E_{pit}).

The crevice corrosion rate values of Steel 4 are maximum at the δ -ferrite content of 65–70 vol.% (3–4 g/m²·h), then with an increase in the δ -ferrite content to 80 vol.% the corrosion rate drops rapidly to near zero values. This steel has the highest PREN and is also Nb-rich with about 0.1 wt.% of Nb. Because of this, Steel 4 is susceptible to the formation of secondary phases—Laves phases and carbonitrides [27]. However, with an increase in quenching temperature, their volume fraction decreases. Therefore, with distance the point of equilibrium of δ -ferrite and austenite on phase diagram, the resistance to crevice corrosion increases.

The crevice corrosion rate values of Steel 5 have the opposite tendency compared to Steel 4. With an increase in the amount of δ -ferrite from 45 to 70 vol.%, the crevice corrosion rate rapidly increases from near zero values to 3 g/m²·h.

Despite the similarities in mechanisms of the pitting and crevice corrosion damage initiation the results of evaluating the corrosion resistance of the Steels show completely opposite results. Steels 1, 2, and 3 showed a smooth growth of the crevice corrosion rate with an increase in the δ -ferrite content from 38 to 100 vol.%. E_{pit} values changes extremely with the highest value at 70 vol.% of δ -ferrite. For Steels 4 and 5 E_{pit} values are at maximum for 50 vol.% of δ -ferrite and gradually decrease farther from the point of equal ratio of ferrite and austenite on phase diagram.

The pitting potential (E_{pit}) for all steels is determined by the alloying level (PREN). Thus, the pitting potentials of steels with high PREN (Steels 4 and 5) are around 1000 mV, but for steels with low PREN (Steels 1, 2, and 3) it is lower: 100–500 mV. Analysis of steels with close PREN values shows that the E_{pit} values also depends on the structural state.

Thus, it is necessary to search for the optimal phase ratio of δ -ferrite and austenite for each grade of DSSs. An equal ratio is not always the optimum.

3.3. Mechanical Properties

Along with a change in the phase composition, a change in mechanical properties occurs. Figure 7 shows the correlation of the hardness and the content of δ -ferrite in steel. Steel with 100 vol.% of δ -ferrite has the highest hardness at 290 HV. As ductile austenite [27] appears in the structure, the hardness gradually decreases to 230 HV at 38 vol.% of δ -ferrite.

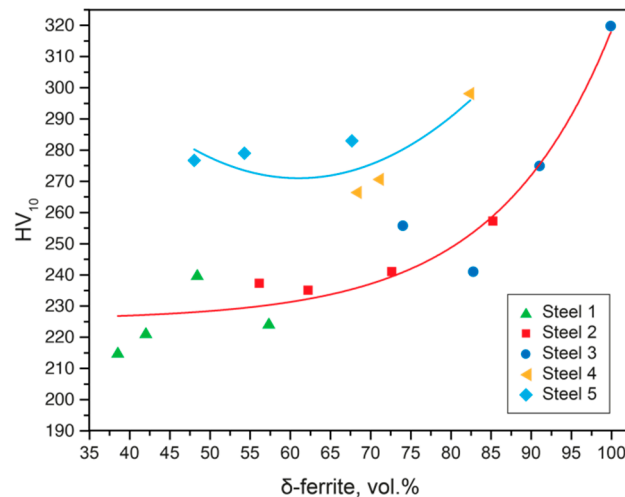


Figure 7. Correlation of hardness HV and the amount of δ -ferrite in steel microstructure.

In steels with the same ferrite content but with different PREN values (different degrees of alloying), the hardness was different. The hardness of Steel 3 with 70 vol.% of δ -ferrite is 230 HV, while the higher-alloy Steel 4 has a hardness of 270 HV with the same δ -ferrite content.

4. Conclusions

A technique for quantitative assessment of the DSS's microstructure based on etching with the Beraha's reagent and subsequent automated analysis has been developed and tested, including the assessment of phase components (austenite and δ -ferrite, σ -phase), secondary phases (carbonitrides and Laves phases), and non-metallic inclusions. Analysis of many other etchants showed that they are not suitable for the investigated steels.

It was shown that the developed technique for quantitative assessment makes it possible to adequately detect secondary phases, carbonitrides, and Laves phases to predict their negative effect on corrosion properties.

The composition of the phases in the specimens was determined using a SEM. The phases were identified and compared with the structure observed with an optical light microscope.

It was shown that the results of measurements after etching with Beraha's reagent correlates well with thermodynamic calculations. It is possible to use the developed technique as a basis for the development of new compositions and technology to produce DSSs.

It was found that the optimal corrosion properties of DSSs are determined not only by the ratio of austenite and ferrite, but by the whole complex of the studied factors. Therefore, depending on the content of secondary phases and non-metallic inclusions, the best corrosion properties can be achieved with different ratios of austenite and ferrite.

It was shown that for all studied DSSs with an increase in the ferrite volume fraction, the steel hardness increases, but its absolute values are different for steels with different alloying levels.

Further results accumulation of the DSSs microstructure analysis, mechanical and corrosion tests will make it possible to develop reasonable requirements for their quality assessment.

Author Contributions: Conceptualization, A.S.F. and A.I.Z.; methodology, A.S.F. and D.A.S.; software, A.I.Z. and A.A.K.; validation, A.S.F., A.I.Z. and A.A.K.; formal analysis, A.A.K.; writing—original draft preparation, A.S.F.; writing—review and editing, A.I.Z. and A.A.K.; visualization, A.S.F.; project administration, A.A.A.; funding acquisition, A.A.A. All authors have read and agreed to the published version of the manuscript.

Funding: The research is partially funded by the Ministry of Science and Higher Education of the Russian Federation as part of World-class Research Center program: Advanced Digital Technologies (contract No. 075-15-2020-934 dated 17 November 2020).

Institutional Review Board Statement: Not applicable.

Informed Consent Statement: Not applicable.

Data Availability Statement: Not applicable.

Conflicts of Interest: The authors declare no conflict of interest.

References

1. Alkhimenko, A. Corrosion testing of experimental steels for oilfield pipelines. *E3S Web Conf.* **2019**, *121*, 01001. [[CrossRef](#)]
2. Kovalev, M.; Lyashenko, D.; Kurakin, M.; Shakhmatov, A. Failure analysis of radial bearings used in the refining of petroleum products. *E3S Web Conf.* **2019**, *121*, 03003. [[CrossRef](#)]
3. Francis, R.; Byrne, G. Duplex Stainless Steels—Alloys for the 21st Century. *Metals* **2021**, *11*, 836. [[CrossRef](#)]
4. Topolska, S.; Łabanowski, J. Effect of microstructure on impact toughness of duplex and superduplex stainless steels. *J. Achiev. Mater. Manuf. Eng.* **2009**, *36*, 142–149.
5. Escobar, J.D.; Faria, G.A.; Maia, E.L.; Oliveira, J.P.; Boll, T.; Seils, S.; Ramirez, A.J. Fundamentals of isothermal austenite reversion in a Ti-stabilized 12Cr–6 Ni–2 Mo super martensitic stainless steel: Thermodynamics versus experimental assessments. *Acta Mater.* **2019**, *174*, 246–259. [[CrossRef](#)]
6. Cojocaru, E.M.; Raducanu, D.; Nocivin, A.; Cinca, I.; Vintila, A.N.; Serban, N.; Cojocaru, V.D. Influence of Aging Treatment on Microstructure and Tensile Properties of a Hot Deformed UNS S32750 Super Duplex Stainless Steel (SDSS) Alloy. *Metals* **2020**, *10*, 353. [[CrossRef](#)]
7. Escobar, J.D.; Poplawsky, J.D.; Faria, G.A.; Rodriguez, J.; Oliveira, J.P.; Salvador, C.A.F.; Ramirez, A.J. Compositional analysis on the reverted austenite and tempered martensite in a Ti-stabilized supermartensitic stainless steel: Segregation, partitioning and carbide precipitation. *Mater. Des.* **2018**, *140*, 95–105. [[CrossRef](#)]
8. Davanageri, M.B.; Narendranath, S.; Kadoli, R. Influence of heat treatment on microstructure, hardness and wear behavior of super duplex stainless steel AISI 2507. *Am. J. Mater. Sci.* **2015**, *5*, 48–52. [[CrossRef](#)]
9. Forgas Júnior, A.; Otubo, J.; Magnabosco, R. Ferrite quantification methodologies for duplex stainless steel. *J. Aerosp. Technol. Manag.* **2016**, *8*, 357–362. [[CrossRef](#)]
10. Escobar, J.D.; Faria, G.A.; Wu, L.; Oliveira, J.P.; Mei, P.R.; Ramirez, A.J. Austenite reversion kinetics and stability during tempering of a Ti-stabilized supermartensitic stainless steel: Correlative in situ synchrotron x-ray diffraction and dilatometry. *Acta Mater.* **2017**, *138*, 92–99. [[CrossRef](#)]
11. ASTM E112-13. *Standard Test Methods for Determining Average Grain Size*; ASTM International: West Conshohocken, PA, USA, 2013. [[CrossRef](#)]
12. ASTM E45-18a. *Standard Test Methods for Determining the Inclusion Content of Steel*; ASTM International: West Conshohocken, PA, USA, 2018. [[CrossRef](#)]
13. ASTM E1268-19. *Standard Practice for Assessing the Degree of Banding or Orientation of Microstructures*; ASTM International: West Conshohocken, PA, USA, 2019. [[CrossRef](#)]
14. Kazakov, A.A.; Zhitenev, A.I.; Fedorov, A.S.; Fomina, O.V. Development of duplex stainless steels Compositions. *CIS Iron Steel Rev.* **2019**, *18*, 20–26. [[CrossRef](#)]
15. Martins, M.; Casteletti, L.C. Sigma phase morphologies in cast and aged super duplex stainless steel. *Mater. Charact.* **2009**, *60*, 792–795. [[CrossRef](#)]
16. Andersson, J.O.; Helander, T.; Höglund, L.; Shi, P.; Sundman, B. Thermo-Calc & DICTRA, computational tools for materials science. *Calphad* **2002**, *26*, 273–312. [[CrossRef](#)]
17. Kovalev, M.; Alkhimenko, A.; Shakhmatov, A. Electrochemical studies of welded joints corrosion resistance made from stainless steels. *Mater. Today Proc.* **2020**, *30*, 501–505. [[CrossRef](#)]
18. Michalska, J.; Sozańska, M. Qualitative and quantitative analysis of σ and χ phases in 2205 duplex stainless steel. *Mater. Charact.* **2006**, *56*, 355–362. [[CrossRef](#)]

19. Llorca-Isern, N.; López-Luque, H.; López-Jiménez, I.; Biezma, M.V. Identification of sigma and chi phases in duplex stainless steels. *Mater. Charact.* **2016**, *112*, 20–29. [[CrossRef](#)]
20. Fedorov, A.; Zhitenev, A.; Strekalovskaya, D. Effect of heat treatment on the microstructure and corrosion properties of cast duplex stainless steels. *E3S Web Conf.* **2021**, *225*, 01003. [[CrossRef](#)]
21. Vander Voort, G.F.; Manilova, E.P. Hints for imaging phases in steels. *Adv. Mater. Process.* **2005**, *163*, 32–37.
22. ASTM A1084-15a. *Standard Test Method for Detecting Detrimental Phases in Lean Duplex Austenitic/Ferritic Stainless Steels*; ASTM International: West Conshohocken, PA, USA, 2015. [[CrossRef](#)]
23. Calliari, I.; Zanesco, M.; Bassani, P.; Ramous, E. Analysis of secondary phases precipitation in duplex stainless steels. *JOM* **2009**, *61*, 80–83. [[CrossRef](#)]
24. ASTM E562-19e1. *Standard Test Method for Determining Volume Fraction by Systematic Manual Point Count*; ASTM International: West Conshohocken, PA, USA, 2019. [[CrossRef](#)]
25. Magnabosco, R. Kinetics of sigma phase formation in a duplex stainless steel. *Mater. Res.* **2009**, *12*, 321–327. [[CrossRef](#)]
26. Sui, S.; Li, Z.; Zhong, C.; Zhang, Q.; Gasser, A.; Chen, J.; Bi, G. Laves phase tuning for enhancing high temperature mechanical property improvement in laser directed energy deposited Inconel 718. *Compos. Part B Eng.* **2021**, *215*. [[CrossRef](#)]
27. Li, J.; Wu, T.; Riquier, Y. δ phase precipitation and its effect on the mechanical properties of a super duplex stainless Steel. *Mater. Sci. Eng. A* **1994**, *174*, 149–156. [[CrossRef](#)]